

Cyclic Testing of Reinforced Concrete Walls with Distributed Minimum Vertical Reinforcement

Yiqiu Lu¹; Richard S. Henry²; Ronald Gultom³; and Quincy T. Ma⁴

Abstract: During the 2010/2011 Canterbury earthquakes in New Zealand, several reinforced concrete (RC) walls in multistory buildings formed only a limited number of cracks at the wall base with a fracture of vertical reinforcement observed. Recent research suggests that walls designed with minimum vertical reinforcement in accordance with current New Zealand standards may not exhibit large ductility during earthquakes. To investigate this theory further, a total of six flexure dominant RC walls with two layers of distributed vertical reinforcement in accordance with minimum requirements were tested. The test walls were typical of multistory RC walls in regions with moderate seismicity in New Zealand and were used to examine the effect of shear span ratio, axial load, and reinforcement ties in the wall end region. The experimental results confirmed that the current minimum vertical reinforcement limits are insufficient to ensure that a large number of secondary flexural cracks will occur in the plastic hinge region. The lateral-load response of the walls was controlled by one or two main large flexural cracks at the wall base. This behavior greatly reduced the spread of plasticity and resulted in several potential issues, such as limited drift capacity and premature reinforcement buckling or fracture. Recommendations are provided related to minimum vertical reinforcement requirements, plastic hinge length assumptions, ultimate drift capacity, and antibuckling reinforcement. DOI: 10.1061/(ASCE)ST.1943-541X.0001723. © 2016 American Society of Civil Engineers.

Author keywords: Reinforced concrete wall; Minimum vertical reinforcement; Seismic design; Plastic hinge length; Drift capacity; Reinforcement buckling; Reinforcement fracture; Concrete and masonry structures.

Introduction

Reinforced concrete (RC) walls are widely used as lateral force resisting elements in both low and high-rise buildings. Ductile RC walls resist lateral forces imposed on the structure during earthquakes through the formation of a flexural plastic hinge at the wall base. The ductility and deformation capacity in the plastic hinge region results from inelastic behavior, including cracking and crushing of concrete and yielding of vertical reinforcement. The rotational capacity of the plastic hinge is dependent on the distribution of cracking, with a greater number of flexural cracks allowing the vertical reinforcement to yield over a significant length. Therefore, to achieve a high ductility capacity during earthquakes, RC walls should be designed to form a large number of distributed primary and secondary flexural cracks in the plastic hinge region, as shown in Fig. 1(a). Primary cracks occur as a result of the flexural cracking strength of the wall being exceeded, whereas secondary cracks occur based on the local tensile stresses induced by the reinforcement into the surrounding concrete.

During the 2010/2011 Canterbury earthquakes in New Zealand, several lightly reinforced concrete walls in multistory buildings

formed only a limited number of cracks or single cracks in the plastic hinge region as opposed to the expected distributed cracking (Kam et al. 2011; SESOC 2011; Sritharan et al. 2014). This type of wall behavior was also observed in buildings following the 1985 Chilean earthquake (Wood 1989; Wood et al. 1991). Because of the lack of distributed cracks, the inelastic deformation of the RC walls was concentrated in a significantly reduced plastic hinge length, resulting in the premature fracture of vertical reinforcement, as shown in Figs. 1(b and c). Furthermore, large crack openings at the wall base can cause additional problems, such as large axial elongations, wall sliding, out-of-plane wall instability, and early reinforcement buckling. In response to the observed performance of lightly reinforced concrete walls, the Canterbury Earthquakes Royal Commission (2012) recommended that research be conducted to investigate crack control for RC walls and that changes should be made to the New Zealand Concrete Structures Standard [NZS 3101:2006 (NZS 2006)] to ensure that yielding of reinforcement can extend beyond the immediate vicinity of a single primary crack.

Minimum reinforcement requirements for RC walls are imposed by most concrete design standards worldwide, both to mitigate shrinkage and temperature effects and to prevent nonductile failure modes. If insufficient vertical reinforcement is provided in RC walls, the cracking moment may exceed the nominal flexural capacity of the wall, and sudden loss of strength and failure could occur. Additionally, the tension force generated by the reinforcement may not be sufficient to develop secondary flexural cracks in the surrounding concrete, resulting in a limited number of cracks. Henry (2013) used a moment-curvature analysis to confirm that RC walls with minimum distributed vertical reinforcement in accordance with the current version (Amendment 2) of NZS 3101:2006 may be susceptible to sudden failure unless a significant axial load was applied. This finding was supported by other researchers who highlighted the potential deficiencies of the current minimum vertical reinforcement requirements. For example, Wood

¹Ph.D. Candidate, Dept. of Civil and Environmental Engineering, Univ. of Auckland, Auckland 1010, New Zealand (corresponding author). E-mail: ylu765@aucklanduni.ac.nz

²Senior Lecturer, Dept. of Civil and Environmental Engineering, Univ. of Auckland, Auckland 1010, New Zealand.

³Ph.D. Candidate, Dept. of Civil and Environmental Engineering, Univ. of Auckland, Auckland 1010, New Zealand.

⁴Senior Lecturer, Dept. of Civil and Environmental Engineering, Univ. of Auckland, Auckland 1010, New Zealand.

Note. This manuscript was submitted on March 19, 2015; approved on October 12, 2016; published online on November 30, 2016. Discussion period open until April 30, 2017; separate discussions must be submitted for individual papers. This paper is part of the *Journal of Structural Engineering*, © ASCE, ISSN 0733-9445.

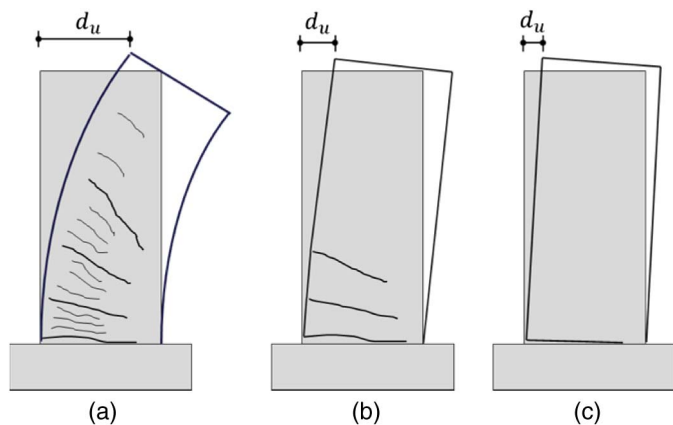


Fig. 1. Crack patterns for ductile and lightly reinforced concrete walls: (a) distributed cracks; (b) limited cracks; (c) single crack

(1989) analyzed the results of 37 RC walls tested prior to 1985 and found that walls with total vertical reinforcement contents less than 1% were susceptible to premature fracture of vertical reinforcement.

Despite research suggesting that current minimum vertical reinforcement limits may be insufficient to ensure well-distributed cracks in plastic hinge regions of multistory ductile walls, only a small number of flexure dominant walls with low vertical reinforcement contents have been tested. For example, Hidalgo et al. (2002) and Greifenhagen and Lestuzzi (2005) tested walls with vertical reinforcement ratios of less than 0.3% and shear span ratios of less than 1. These squat wall tests were designed to investigate shear behavior rather than the flexure-dominant walls typical of multistory buildings. Additionally, Deng et al. (2012) tested four walls with light vertical reinforcement and shear span ratios between 3 and 4. However, these walls were subjected to high axial loads that are not typical of New Zealand buildings. Dazio et al. (2009) tested three walls with vertical reinforcement ratios between 0.39 and 0.54%, and Li et al. (2012) tested eight walls with vertical reinforcement ratios of 0.8%; however, all these walls had concentrated vertical reinforcement at the wall ends, which assisted in the formation of secondary cracking. Limited experimental tests have been conducted on flexure-dominant RC walls with distributed minimum vertical reinforcement and low axial loads that are representative of RC walls in many countries with low or moderate seismicity.

To address the lack of experimental data on flexure-dominant lightly reinforced concrete walls, a series of experimental tests were conducted on RC walls designed with minimum distributed vertical reinforcement. Six RC walls were designed in accordance with NZS 3101:2006 to represent typical multistory walls that are common in low or moderate seismic regions. The six test walls were designed to investigate the effect of shear span ratio, axial

load, and transverse reinforcement ties in the end region on the seismic performance of RC walls with identical vertical reinforcement and material properties. The experimental results, including observed crack pattern, failure mode, and overall hysteric response, are presented, and data from a detailed array of instrumentation are discussed in terms of deformation components, curvature distribution, plastic hinge length, vertical reinforcement strains, reinforcement buckling, cracking moment, and lateral drift capacity.

Experimental Investigation

Test Walls

The experimental program comprised six large-scale rectangular RC walls that were subjected to pseudo-static cyclic loading. A summary of the main parameters for the six test walls is provided in Table 1, and drawings of the wall specimen are shown in Fig. 2. The 1.4 m long, 2.8 m high, and 150 mm thick test walls were designed to approximately represent a 40–50% scale version of multistory flexure-dominant RC walls. The detailing was designed with limited ductile detailing requirements in accordance with NZS 3101:2006. The full-scale prototype wall was expected to have a thickness of 300–375 mm and a length of 2.8–3.5 m, which is comparable to the dimensions of the grid-3 wall in the Gallery Apartments Building in Christchurch (Smith and England 2012). The vertical reinforcement was identical for all six walls and designed using the current minimum requirements in NZS 3101:2006, as shown by Eq. (1) and explained in more detail by Henry (2013). For the test walls, the specified concrete strength (f'_c) was 40 MPa, and the reinforcement yield strength (f_y) was 300 MPa, so the total vertical reinforcement content (ρ_n) in the wall was calculated as 0.53% using Eq. (1), resulting in two layers of seven D10 bars placed at 225 mm centers over the wall length, as shown in Fig. 2.

$$\rho_n \geq \frac{\sqrt{f'_c}}{4f_y} \quad (1)$$

It should be noted that the minimum vertical reinforcement ratio designed in accordance with NZS 3101:2006 is larger than that required by other design standards. ACI 318-14 (ACI 2014) requires a distributed minimum vertical reinforcement ratio of 0.25% for special structural walls and encourages the use of concentrated vertical reinforcement in the ends of the wall, but it does not explicitly state any limits. Eurocode 8 requires a minimum vertical reinforcement ratio of 0.5% in the ends of walls and a distributed minimum vertical reinforcement ratio of 0.2%.

To test multistory building walls in a range of different building heights, three shear span ratios (the ratio of shear span height to wall length) were applied to the test walls, equal to 2, 4, and 6. Accordingly, the shear span ratio applied to the 40–50% scale test

Table 1. Details of All Six Test Walls

Wall	Shear span ratio (M/Vl_w)	Axial load ratio (%)	Shear demand to capacity ratio	Vertical reinforcement ratio (%)	Horizontal reinforcement ratio (%)	End ties
C1	2	3.5	0.42	0.53	0.25	None
C2	4	3.5	0.21	0.53	0.25	None
C3	6	3.5	0.14	0.53	0.25	None
C4	2	0	0.26	0.53	0.25	None
C5	2	6.6	0.53	0.53	0.25	R6 at 90 mm
C6	4	3.5	0.42	0.53	0.25	R6 at 60 mm

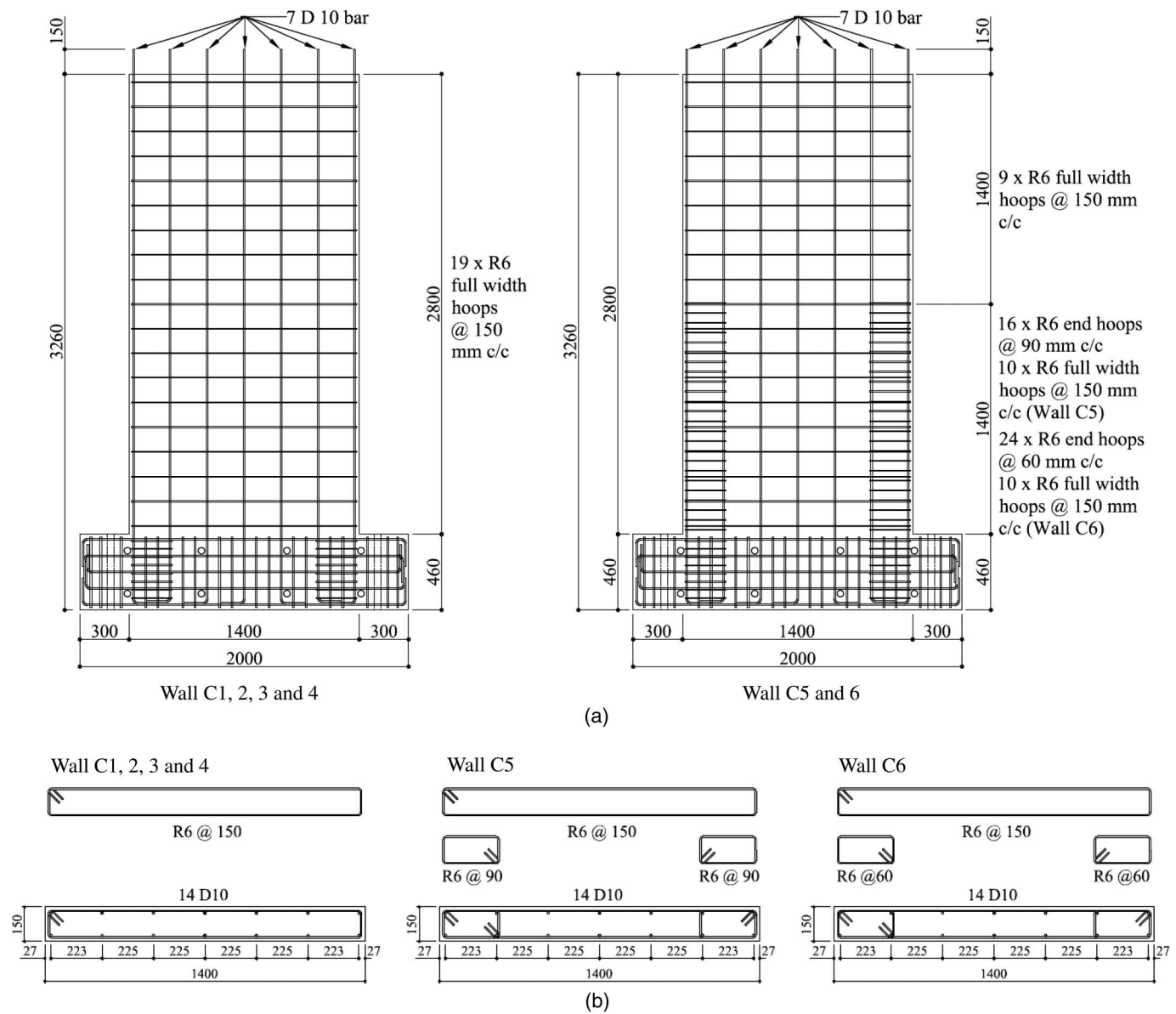


Fig. 2. Details of test wall specimens: (a) elevations; (b) cross sections

walls approximately represented walls in buildings with a height of 8–40 m (2–12 stories). A survey of New Zealand structural engineers indicated that typical axial load ratios ($N/A_g f'_c$) for this type of RC wall ranged from 0 to 10% of the wall axial capacity, with the majority less than 5%. To reflect this practice, the axial load ratios applied to the test walls were equal to 0, 3.5, and 6.6%, which corresponded to actual applied axial loads of 0, 290, and 555 kN, respectively. The shear demand to capacity ratio, defined as the shear at nominal flexural strength (V_{mn}) divided by the nominal shear strength (V_n) calculated in accordance with NZS 3101:2006 and ACI 318-14 (identical), are provided in Table 1. The shear demand to capacity ratio was significantly less than 1 for all test walls, which confirmed that the walls were likely to be flexure dominant. The shear demand index, calculated as V_{mn} divided by $A_{cv} \sqrt{f'_c}$, was also extremely small, ranging from 0.04 to 0.15 for all the test walls. For flexure-dominant walls, a low shear span ratio results in a sharp decrease in the bending moment profile over the wall height, which is expected to contribute to the reduced spread of the plasticity. Therefore, it was considered that a

shear span ratio of 2 was likely to be most critical for lightly reinforced concrete walls and so Test Wall C1 was chosen as the reference wall. As shown in Table 1, Test Walls C1, C2, and C3 varied the shear span ratio between 2, 4, and 6 with a consistent axial load ratio of 3.5%. Walls C4, C1, and C5 were designed to vary the axial load ratio between 0, 3.5, and 6.6% with a consistent shear span ratio of 2. The self-weight of the test walls was not accounted for in the axial load ratios listed earlier.

The horizontal reinforcement was designed following procedures in NZS 3101:2006. Only minimum horizontal reinforcement was required to provide shear capacity, resulting in R6 stirrups distributed evenly at 150 mm centers over the wall height, as shown in Fig. 2. For Walls C1, C2, C3, and C4, no additional transverse reinforcement was required to meet the limited ductility detailing requirements in NZS 3101:2006. The axial loads applied to these four walls were not large enough to trigger requirements for confinement reinforcement, and the vertical reinforcement ratio was too low to require antibuckling ties. The larger axial load ratio of 6.6% applied to Wall C5 did trigger the requirements for

additional confinement reinforcement to achieve a limited ductility response, resulting in R6 stirrups placed in the wall toes at 90 mm centers over the lower 1.4 m of the wall section, as shown in Fig. 2. According to the current version (Amendment 2) of NZS 3101:2006, none of the test walls required antibuckling ties because the vertical reinforcement ratio was less than $3/f_y$. The provisions in ACI 318-14 (ACI 2014) are similar, with antibuckling ties not required unless the vertical reinforcement ratio exceeds $2.76/f_y$. However, in Eurocode 8 (CEN 2004), at least 6 mm antibuckling ties would be required for all the test walls to mitigate local reinforcement buckling. To investigate the requirements for antibuckling restraint in lightly reinforced concrete walls, R6 stirrups were placed in the wall toes at 60 mm centers over the lower 1.4 m of the wall section for Wall C6, as shown in Fig. 2. All other parameters for Wall C6 were identical to those for Wall C2, as indicated in Table 1.

Test Setup

Because of height limitations in the structural test laboratory at the University of Auckland, a test setup was designed to simulate the

expected seismic loading on the lower portion of the scaled RC wall that represented designs appropriate for taller buildings. Based on an assumed lateral-load distribution, a combination of moment, shear, and axial load can be applied to the top of the test wall to simulate seismic loading of taller RC walls, as was previously achieved by numerous researchers (Crisafulli et al. 2002; Han et al. 2002; Brueggen 2009). In addition, the walls were tested as isolated specimens without considering their interaction with the floor diaphragms and other structural systems. To illustrate this load combination, the test setup used for the RC wall test is shown in Fig. 3. An actuator with a force capacity of ± 300 kN and displacement capacity of ± 300 mm was attached between the steel loading beam and the strong wall to apply horizontal loads to the wall, and two additional actuators with a force capacity of ± 300 kN and displacement capacity of ± 150 mm were attached vertically at each end of the wall to achieve the required combination of moment and axial load at the top of the wall. For test walls with a shear span ratio equal to 2, the two vertical actuators applied a constant axial load throughout the test with no moment applied to

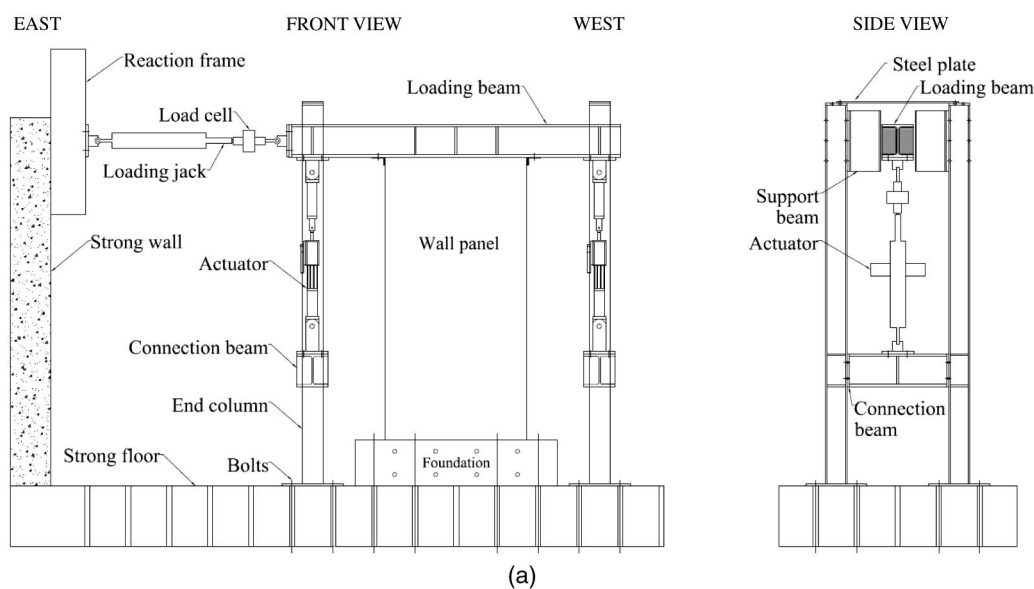


Fig. 3. Test setup used to achieve desired test moment-to-shear ratio: (a) test setup illustration; (b) test setup in lab

the top of the wall. For the test walls with a shear span ratio larger than 2, the two vertical actuators were programmed to apply both a constant axial load and a moment that was calculated based on the output of the horizontal force. A steel frame was designed to support the vertical actuators and to provide lateral restraint to the loading beam to prevent out-of-plane movement, as shown in Fig. 3.

The walls were constructed of a uniform-thickness panel with two foundation blocks located on each side of the wall. The two foundation blocks were 2 m long, 410 mm wide, and 460 mm high and were constructed using a 40 MPa specified concrete strength. The reinforcement in the two foundation blocks consisted of $12 \times$ HD12 500 MPa longitudinal reinforcement and HD10 transverse stirrups placed at 75 mm centers. The wall panel was made 2 m long at the foundation part to match the length of the two foundation blocks. A 15 mm gap between the two foundation blocks and the wall panel on both sides was grouted using 40 MPa strength grout prior to posttensioning the wall panel and the two foundation blocks together, and to the laboratory strong floor, to create an equivalent monolithic foundation. This method of constructing the foundation block did not significantly affect the outcome of the test results during the test when compared to a cast-in-place foundation. The vertical reinforcement in the wall extended out of the top of the wall and was secured to the steel loading beam using steel tube anchor blocks filled with 80 MPa (28-day specified strength) grout around each bar.

Loading Protocol

The loading protocol applied to the test walls was developed in accordance with ACI 374.2R-13 (ACI 2013) and ACI ITG-5.1-07 (ACI 2008). Prior to applying the cyclic lateral load, the axial load was applied via the two vertical actuators and kept constant throughout the testing. The first four lateral-load cycles were force-controlled with load increments equal to one-fourth,

one-half, three-fourths, and one times the force corresponding to the theoretical cracking moment at the wall base calculated using the average expected concrete strength. The following cycles were drift-controlled with three full cycles at each drift level applied to the wall. Drift values for the subsequent three cycles to a new maximum lateral drift were to values not less than five-fourths times and not more than three-halves times the previous maximum lateral drift. This resulted in drift-controlled cycles of 0.2, 0.25, 0.35, 0.5, 0.75, 1.0, 1.5, 2.0, and 2.5% lateral drift.

Instrumentation

The test walls' response was monitored using a dense array of instrumentation, as shown in Fig. 4. The horizontal displacement at the top of the wall was measured using two string-pot displacement gauges, and the forces and displacements applied by each actuator were monitored using internal load cells and LVDTs. On one face of the wall, steel studs were embedded in the concrete during construction approximately 30 mm from the wall edges. Displacement gauges were attached to these studs to measure the local deformations of different sections of the wall. A total of nine displacement gauges were placed at each edge up the height of the wall to monitor axial strains and curvatures. Shear deformations in the wall were measured using displacement gauges in X configurations over two panel regions, as shown in Fig. 4. To accurately capture the cracking at the wall base, two rows of five displacement gauges were placed along the wall length and extending 300 mm up the wall height. Steel studs were also welded directly onto the corner vertical reinforcement that passed through recesses in the cover concrete to allow the average reinforcement strains to be measured using external displacement gauges over a 150 mm gauge length. Strain penetration of the vertical reinforcement at the wall–foundation interface was measured using a displacement gauge connected to the bottom stud welded on the vertical reinforcing bar and foundation. Displacement gauges were also

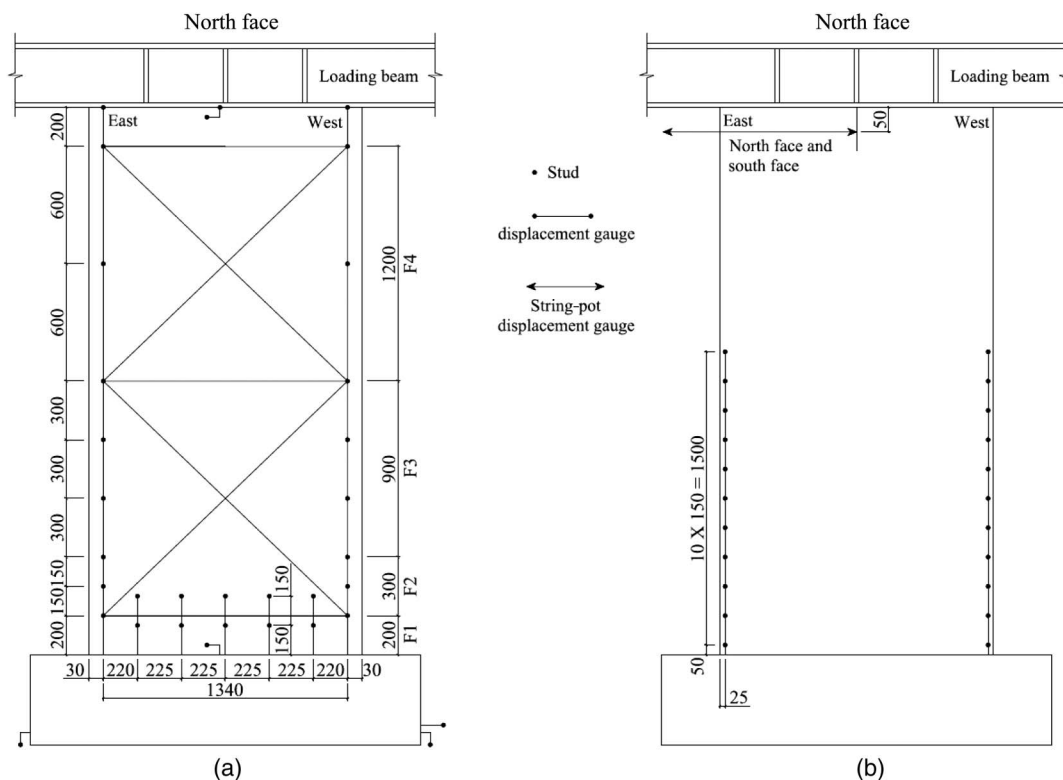


Fig. 4. Instrumentation used for test walls: (a) panel displacement gauges; (b) strain gauges and string pots

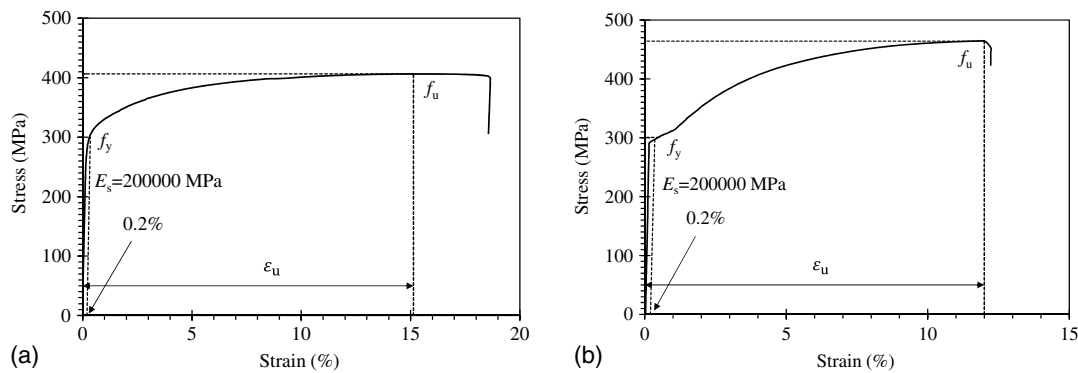


Fig. 5. Typical stress–strain relationship for reinforcement: (a) D10; (b) R6

Table 2. Mechanical Properties of Concrete

Test wall	f'_c (MPa)	E_c (GPa)	f_t (MPa)	ρ_c (kg/m ³)
C1	38.5	26.0	2.88	2,405
C2	34.5	27.5	2.53	2,552
C3	36.2	30.0	3.05	2,391
C4	34.7	26.7	2.65	2,323
C5	35.4	28.3	2.81	2,342
C6	37.3	26.7	2.81	2,369

used to measure any potential vertical and horizontal slip at the wall-to-foundation, wall-to-loading-beam, and foundation-to-strong-floor joints. On the other face of the wall, a random pattern of black dots was painted to trial a digital image correlation system, but the results of these measurements are not presented.

Material Properties

Grade 300E reinforcing steel produced by Pacific Steel Group in accordance with AS/NZS 4671 (AS/NZS 2001) was used in the test walls. Three samples of each type of reinforcing bar were tested to confirm their stress–strain behavior. The average ultimate strain ϵ_u was determined as the uniform elongation over a 100 mm gauge length at maximum stress and equal to 15.3 and 12.6% for the D10 (deformed G300E, diameter = 10 mm) and R6 (plain G300E, diameter = 6 mm) bars, respectively. A typical stress–strain relationship for the D10 and R6 reinforcement is plotted in Fig. 5. Smaller diameter bars are usually stored in coil form, and the yield plateau is lost when the bar is straightened, so the yield strength (f_y) was taken as 0.2% proof force divided by the nominal area of the bar.

Table 3. Key Observations of All Six Test Walls

Test wall	Direction	First cracking (%)	Concrete spalling (%)	Reinforcement buckling (%)	Core concrete crushing (%)	Reinforcement fracture (%)
C1	+	+0.20	+1.0 ^{3a}	+1.5 ¹	N/A	+2.5 ³
	–	–0.20	–1.0 ³	–1.5 ¹	–2.0 ¹	N/A
C2	+	+0.06	+1.5 ³	+1.5 ³	+2.0 ³	+2.5 ³
	–	–0.06	–1.5 ¹	–1.5 ³	–2.0 ³	–2.5 ³
C3	+	+0.16	+1.5 ¹	+1.5 ³	+2.0 ³	+2.5 ²
	–	–0.16	–1.0 ³	–1.0 ³	–2.0 ³	–2.5 ²
C4	+	+0.06	+0.75 ²	+1.0 ¹	+1.0 ³	+1.5 ³
	–	–0.06	–0.75 ¹	–0.75 ²	N/A	–1.5 ¹
C5	+	+0.20	+1.5 ³	+1.5 ³	+2.5 ¹	+2.0 ³
	–	–0.20	–1.5 ¹	–1.5 ¹	–2.0 ³	–2.0 ²
C6	+	+0.12	+1.0 ³	+1.5 ³	N/A	+2.5 ³
	–	–0.12	–2.0 ¹	–2.0 ³	N/A	–2.0 ²

^aThe superscript denotes the cycle number; + signifies drift to west; – signifies drift to east.

The average yield and ultimate strength for D10 were 300 and 409 MPa, respectively. For R6, the average yield and ultimate strength were 300.6 and 461.8 MPa, respectively.

The measured mechanical properties of the concrete at the time of testing each of the six walls are listed in Table 2. Six concrete cylinders with a diameter of 100 mm and a height of 200 mm were made from the same batch of concrete and cured alongside each wall panel in ambient conditions, with three cylinders being used for compression tests and the other three for split cylinder tests to estimate the tensile strength (f_t). It should be noted that the tensile strengths presented in Table 2 are average splitting tensile strengths calculated directly from the test conducted in accordance with NZS 3112.2 (NZS 1986). The modulus of elasticity (E_c) was determined as the secant stiffness from the origin to 50% of the peak concrete compressive strength.

Test Observations and Results

Table 3 provides a summary of the drift cycle during which key observations were made during the tests, including first cracking, concrete spalling, reinforcement buckling, core concrete crushing, and reinforcement fracture. In the following section, a brief description of the evolution of the wall behavior is given for each of the test walls. An example of the typical test wall condition is shown for Wall C1 in Fig. 6. The crack patterns and the maximum measured crack widths at the end of the test of six test walls are shown in Fig. 7. The crack patterns visible on both the north and south sides of the wall were similar, with minor differences as the cracks propagated through the wall. Therefore, the crack patterns in Fig. 7 were drawn only from the southern side, where the left-hand end is west and the right-hand end is east. The final condition of each of

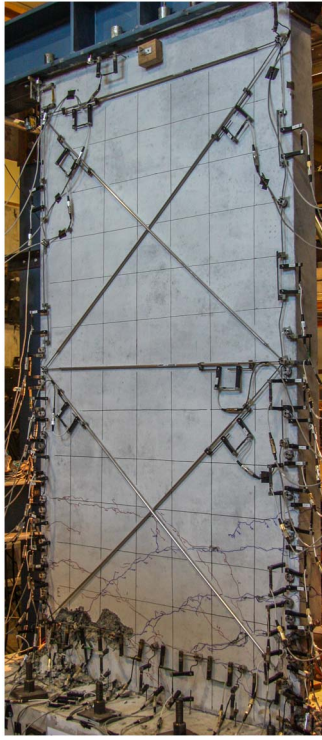


Fig. 6. Overall condition of Wall C1 at end of test

the walls is shown in Fig. 8, and the moment-displacement hysteresis response for all six test walls is shown in Fig. 9. The foundation behaved similarly to an equivalent monolithic foundation, with no damage observed during any of the tests. The grouted interface and posttensioning was sufficient to transfer the wall forces to the foundation blocks with no slip occurring.

Wall C1

Wall C1 was considered the baseline wall with a shear span ratio of 2 and axial load ratio of 3.5%. The wall response was dominated by flexural behavior with three or four main flexural cracks forming in the lower one-fourth of the wall height, as shown in Figs. 6 and 7(a). These three or four primary flexural cracks all initiated prior to a lateral drift of $\pm 0.25\%$, after which no significant new flexural cracks occurred during the test. During larger lateral drift cycles, the wall deformation was primarily concentrated at one large flexural crack at the wall base, which opened up to 20 mm wide, with the other flexural cracks not opening wider than a few millimeters. However, despite the large crack width at the wall base, no significant shear sliding was recorded. The concrete at the corners of the wall started to spall during the cycles at lateral drifts of $\pm 1.0\%$, and buckling of the vertical reinforcement initiated at the location of the largest flexural crack during cycles at lateral drifts of $\pm 1.5\%$. As shown in Table 3, the drift levels at key observations were slightly different between positive and negative directions owing to the different crack patterns and crack widths observed at the two ends of the wall. Because of the lack of confinement reinforcement, buckling of the vertical reinforcement accelerated concrete spalling, and core crushing occurred during the first cycle at -2.0% drift. The two corner reinforcing bars at the east end of the wall fractured during the third cycle at $+2.5\%$ drift, as shown in Fig. 8(a). As shown in Fig. 9(a), the uncracked wall had a high initial cross-sectional stiffness, and the first flexural crack initiated at a wall base moment of 332.5 kN-m, or roughly 68% of the peak

strength. The test wall stiffness and strength deteriorated slightly during the second and third cycles at each drift level, which was consistent with other RC wall tests (Dazio et al. 2009; Lowes et al. 2012). The strength increased slightly when the wall was subjected to a new drift level until 1.5% lateral drift, when buckling of the vertical reinforcement occurred, after which a deterioration in strength occurred on each cycle at a new drift level. A drop of 20% of the peak strength occurred when the core was crushed during the first cycle at -2.5% lateral drift. The strength degradation continued, and two of the vertical reinforcing bars fractured during the third cycle at $+2.5\%$ lateral drift. The test was terminated after three cycles at $\pm 2.5\%$ lateral drift.

Wall C2

Test Wall C2 was identical to Wall C1, except that the shear span ratio was increased from 2 to 4, meaning that a moment was applied to the top of the wall in addition to the lateral force. As a result of the higher shear span ratio, the flexural cracks extended higher up the height of Wall C2, as shown in Fig. 7(b). However, the wall response was still dominated by three or four large flexural cracks at the wall base, with other cracks less than 2 mm wide. As with Wall C1, all the flexural cracks formed prior to 0.5% lateral drift, and no significant shear-sliding was recorded during the test. The concrete in the east corner started to spall during the first cycle at -1.5% lateral drift, and buckling of the vertical reinforcement initiated at the wall base during the third cycle at $\pm 1.5\%$ lateral drift. During the cycles at $\pm 2.0\%$ lateral drift, the reinforcement buckling became more severe and crushing of the core concrete occurred. Two corner vertical reinforcing bars at the east end of the wall fractured during the third cycle at $+2.5\%$ lateral drift, as shown in Fig. 8(b), and one reinforcing bar fractured at the west end of the wall during the third cycle at -2.5% lateral drift. As shown in Fig. 9(b), the measured moment-displacement response for Wall C2 was similar to that of Wall C1. The first flexural crack initiated during the first cycle at -0.06% lateral drift at a wall base moment of 352.9 kN · m, or roughly 65% of the peak strength. The inelastic response of Wall C2 was stable up to $\pm 1.5\%$ lateral drift, when buckling of the vertical reinforcement occurred and caused a gradual degradation in wall strength. Two vertical reinforcing bars fractured during the third cycle at $+2.5\%$ lateral drift, leading to a 20% drop in peak strength. During the third cycle at lateral drift of -2.5% , the wall also experienced a large drop in strength due to the fracture of more vertical reinforcement.

Wall C3

Wall C3 was identical to Walls C1 and C2, except that loading was applied to generate a higher shear span ratio of 6. As shown in Fig. 7(c), the cracks extended over almost the entire wall height. Although a large number of cracks formed, the spacing of these cracks was generally greater than 200 mm, and no significant secondary cracking occurred between these primary flexural cracks. Like the behavior of Wall C2, that of Wall C3 was controlled by three or four main flexural cracks at the wall base, and again no significant shear sliding was recorded during the test. Concrete spalling and buckling of vertical reinforcement were observed at the east end of the wall during the third cycle at -1.0% lateral drift. It should be noted that concrete spalling occurred at similar drifts for Walls C1, C2, and C3 and was not significantly affected by the shear span ratio. This observation was attributed to the fact that concrete crushing occurred as a secondary effect following buckling of the vertical reinforcement. The neutral axis depth was not sufficient to induce large compressive strain due

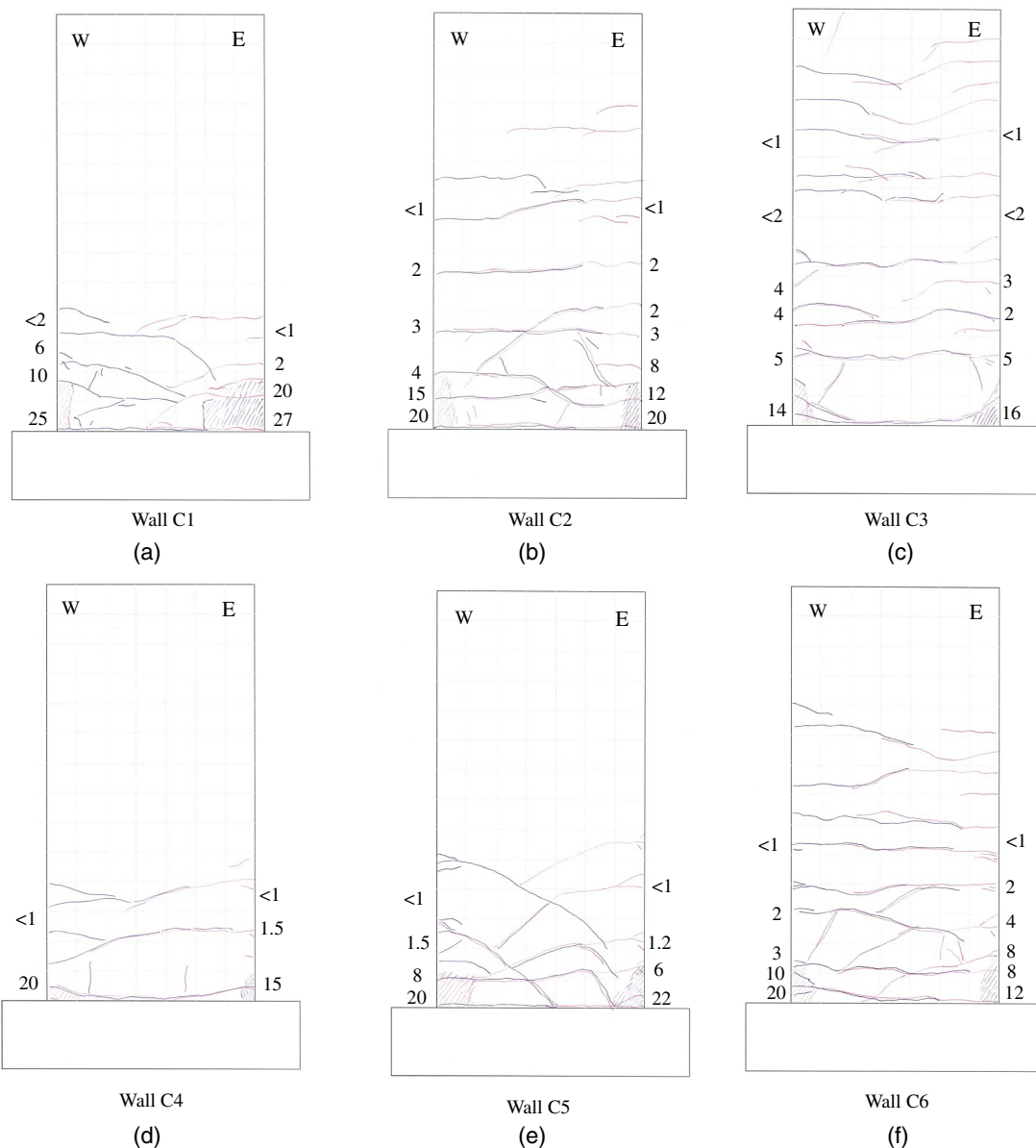


Fig. 7. Final crack patterns and maximum measured crack widths of six test walls (in millimeters): (a) Wall C1; (b) Wall C2; (c) Wall C3; (d) Wall C4; (e) Wall C5; (f) Wall C6

to the low reinforcement content. Therefore, the drift capacity and wall behavior was primarily dependent on reinforcement tensile strains and buckling rather than the increase in bending moment up the wall height. During the cycles at $\pm 2.0\%$ lateral drift, reinforcement buckling became more severe and the core concrete started to crush at the east end. One vertical reinforcing bar at the east end of the wall fractured during the second cycle at $+2.5\%$ lateral drift, as shown in Fig. 8(c), and one vertical reinforcing bar at the west end of the wall fractured during the second cycle at -2.5% lateral drift. The measured moment-displacement response for Wall C3 shown in Fig. 9(c) was similar to the response observed for Walls C1 and C2. A few flexural cracks initiated simultaneously during the first cycle at a drift of $+0.16\%$ at a wall base moment of $354.4 \text{ kN} \cdot \text{m}$, or 64% of the peak strength. Strength degradation again occurred after $\pm 1.5\%$ lateral drift due to reinforcement buckling, and the strength dropped below 80% of the peak strength owing to reinforcement fracturing during the second cycle at -2.5% lateral drift. From the results of the tests

on Walls C1, C2, and C3, the shear span ratio did not appear to have a significant effect on the drift capacity of the test walls.

Wall C4

Wall C4 was comparable to Wall C1, but it was subjected to zero axial load. Only three flexural primary cracks were observed in the bottom one-fourth of Wall C4, with the bottom crack opening to a width greater than 20 mm and the other two cracks less than 1.5 mm wide. These cracks all initiated before 0.25% lateral drift and no other cracks occurred until the end of the test. The concrete started to spall during the second cycle at $\pm 0.75\%$ lateral drift. Two corner vertical reinforcing bars at the east end of the wall buckled during the second cycle at -0.75% lateral drift, which was much earlier than the walls with axial loads applied. At the west end, the vertical reinforcement buckled during the first cycle at $+1.0\%$ lateral drift. Two corner reinforcing bars and one web vertical reinforcing bar at the east end of the wall fractured during the third

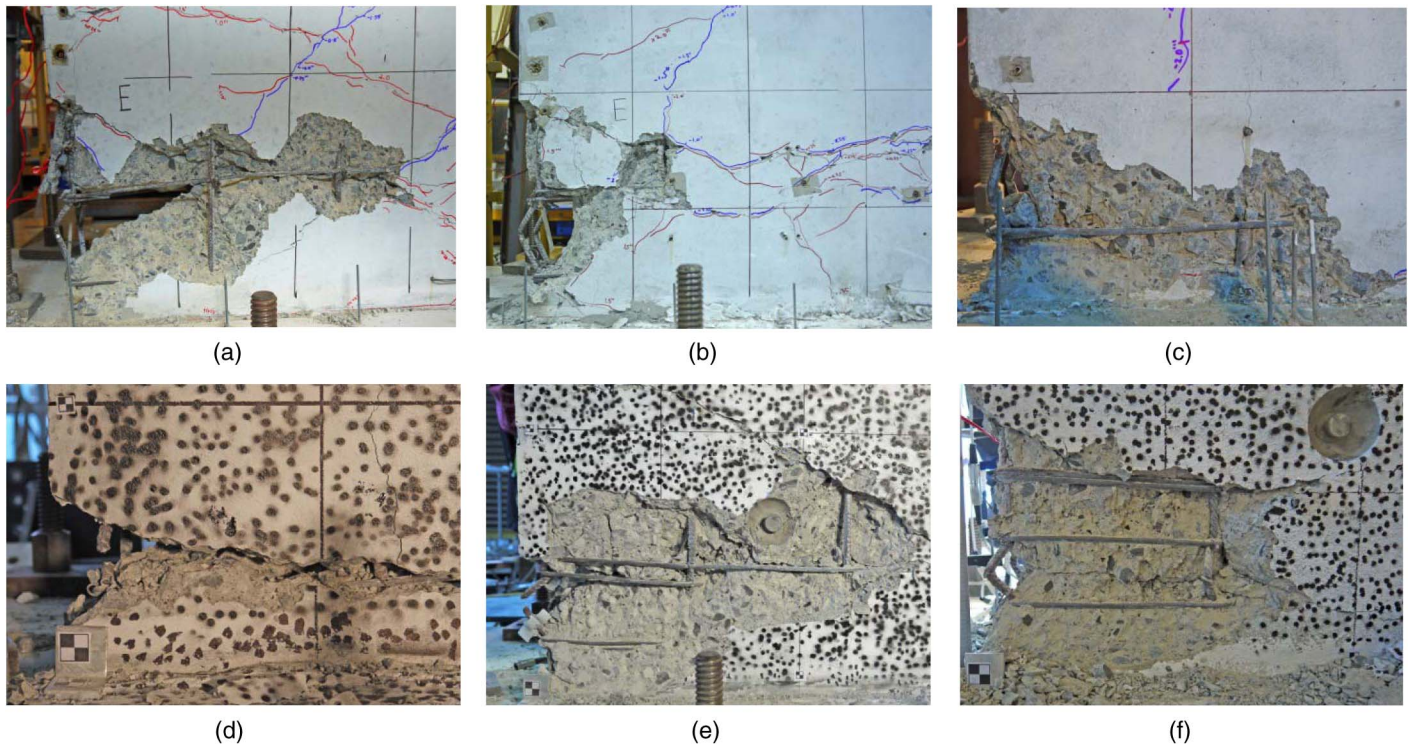


Fig. 8. Wall toe at end of each test: (a) Wall C1; (b) Wall C2; (c) Wall C3; (d) Wall C4; (e) Wall C5; (f) Wall C6

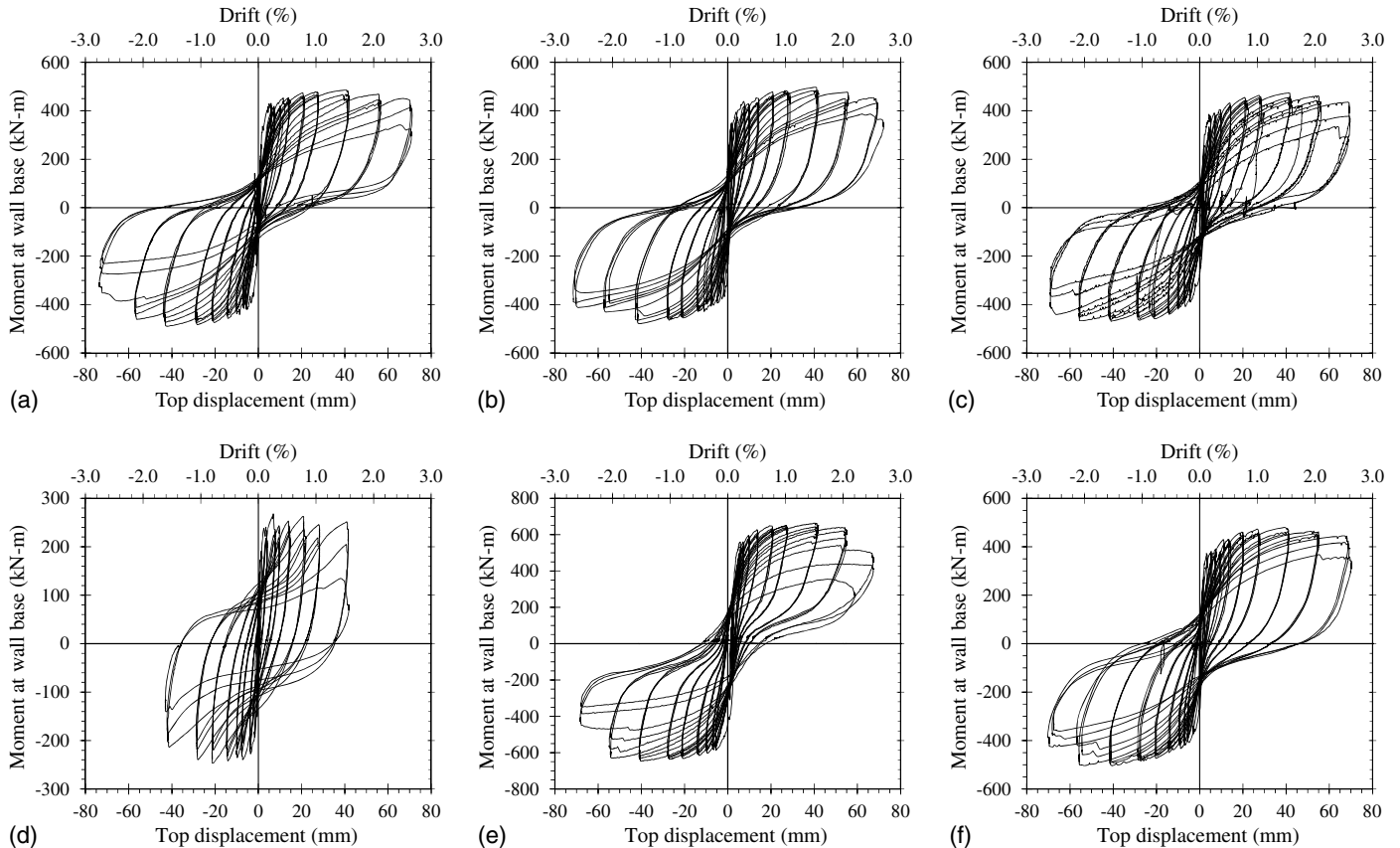


Fig. 9. Moment-displacement response for all six test walls: (a) Wall C1; (b) Wall C2; (c) Wall C3; (d) Wall C4; (e) Wall C5; (f) Wall C6

cycle at +1.5% lateral drift. Core concrete started to crush in the west corner during the third cycle at +1.0% lateral drift, and the buckled reinforcement fractured during the first cycle at -1.5% lateral drift, as shown in Fig. 8(d). As Wall C4 had no axial load applied, the shape of the measured moment-displacement response was significantly different from that of the other walls that had an axial load, as shown in Fig. 9(d). In addition, the measured moment-displacement response also indicated that the wall experienced shear sliding in the later stages of the test because of the large continuous crack at the wall base that did not close when the load was removed owing to the absence of additional axial load. The first crack was observed at a wall base moment of 169.5 kN · m, or 63% of the peak strength. The strength dropped below 80% of the peak strength during cycles at -1.5% lateral drift due to the fracture of three reinforcing bars at the east end. The test of Wall C4 confirmed that the absence of axial load resulted in a poor behavior and reduced drift capacity when compared to previous tests with 3.5% axial load.

Wall C5

Wall C5 was comparable to Wall C1, but the axial load ratio was increased to 6.6%. The crack pattern was similar to that in Wall C1, with three or four main flexural cracks, and the deformation was also controlled by one or two wide cracks at the wall base. Because of the higher axial load, the lateral strength of the wall increased and caused more obvious diagonal shear cracks in the wall. Owing to the high axial load, shear sliding was negligible throughout the test. Concrete spalling and buckling of the vertical reinforcement occurred at both ends of the wall during cycles at $\pm 1.5\%$ lateral drift. Two reinforcing bars at the west end of the wall fractured at the second and third cycle at -2.0% lateral drift, respectively. At the east end, one reinforcing bar fractured during the third cycle at +2.0% lateral drift, and the other corner reinforcing bar fractured during the first cycle at +2.5% lateral drift. Despite the use of confinement reinforcement in the wall ends, the core concrete crushed severely and the web vertical reinforcing bars also buckled at the later stages of the test, as shown in Fig. 8(e). The measured moment-displacement response for Wall C5 in Fig. 9(e) was flag shaped owing to the high axial load and low vertical reinforcement content. Several flexural cracks initiated during the first cycle at -0.2% lateral drift at a wall base moment of 415.4 kN · m, or roughly 63% of the peak strength. As with Wall C1, the inelastic response was stable up until $\pm 1.5\%$ drift when reinforcement buckling occurred and caused a gradual degradation in wall strength. Fracture of the reinforcement at the west end of the wall led the strength to drop below 80% of the peak strength during the third cycle at a drift of -2.0%, and the wall also experienced a large drop in strength during the first cycle at a drift of +2.5% owing to reinforcing bar fracture. Concrete crushing due to the high axial load caused the wall to experience a significant drop in strength during cycles at $\pm 2.5\%$ drift.

Wall C6

Wall C6 was identical to Wall C2, except that antibuckling reinforcement was provided in the form of closely spaced stirrups in the end region of wall. As shown in Fig. 7(f), the observed crack pattern for Wall C6 was similar to that observed for Wall C2. The flexural cracks extended over approximately three-fourths of the wall height, with three or four dominant cracks at the wall base. No significant shear sliding was recorded during the test. Despite the presence of the antibuckling reinforcement, the onset of concrete spalling and buckling of the vertical reinforcement was still

observed at the west end of the wall during the third cycle at 1.5% lateral drift. The two buckled reinforcing bars fractured during the second and third cycles at a drift of 2.0%, causing a large drop in lateral strength. Concrete spalling occurred at the east end of the wall during the first cycle at -2.0% lateral drift, but there was no sign of reinforcement buckling until the third cycle at -2.0% drift. The buckled reinforcing bar at the east end fractured during cycles at -2.5% lateral drift, leading to a 20% drop in peak strength. The final condition on the west end of the wall is shown in Fig. 8(f). The measured moment-displacement response for Wall C6 shown in Fig. 9(f) was similar to that of Wall C2. Two flexural cracks initiated at a wall base moment of 334.9 kN · m, or roughly 70% of the peak strength. The strength started to drop during cycles at 1.5% lateral drift when the wall was pushed to the west, while in the other direction the wall maintained a stable response until -2.0% lateral drift when reinforcement buckling occurred. The ultimate drift of 2.5% for Wall C6 was the same as that observed for Wall C2, indicating that the transverse reinforcement in the end region had little effect on the wall drift capacity.

Discussion of Test Results

The instrumentation used allowed both the global and local response of the test walls to be investigated. The data are interpreted in the following sections in terms of deformation components, curvature distribution, plastic hinge length, reinforcement strains, reinforcement buckling, cracking moment, and drift capacity.

Deformation Components

To investigate the deformation contributions of different sections of the wall panel, the wall was split into four components, F1, F2, F3, and F4, as shown in Fig. 4(a). The flexural deformations were calculated by double-integrating the curvatures calculated from vertical displacement gauges along both wall edges, assuming plane sections remain plane. The shear deformations were computed directly from the diagonal displacement gauges in accordance with the methods proposed by Hiraishi (1984). The shear deformations in the six test walls were small, and their effect on vertical displacement gauges was therefore negligible. The wall lateral displacement due to reinforcement strain penetration at the wall-foundation interface was difficult to quantify because the test walls were dominated by two to three main flexural cracks, and the strain penetration could not be separated from the wide crack at the wall base. Therefore, the lateral displacement resulting from reinforcement strain penetration was not calculated separately but was instead included in the flexural component F1. The contributions of the five displacement components during the first cycle to each lateral drift target are shown for each test wall in Fig. 10. The summation of these five displacement components correlated well with the wall displacement measured directly using string-pot displacement gauges, with an error typically less than 10%.

For all six walls, the flexural displacements were considerably larger than the shear displacements, which typically accounted for less than 5% of the total lateral displacement. Even for Wall C1, with a shear span ratio of 2, the wall was extremely flexure dominant and the shear deformations observed were significantly less than those recorded in other ductile RC wall tests, such as walls tested by Lowes (2012) (shear span ratio = 2.85 or 2.0, shear deformation around 20%) and Dazio et al. (2009) (shear span ratio = 2.28 or 2.26, shear deformation around 10%). In addition, the flexural deformations in the bottom portion of the wall panel contributed the majority of the wall lateral deformation. For Wall

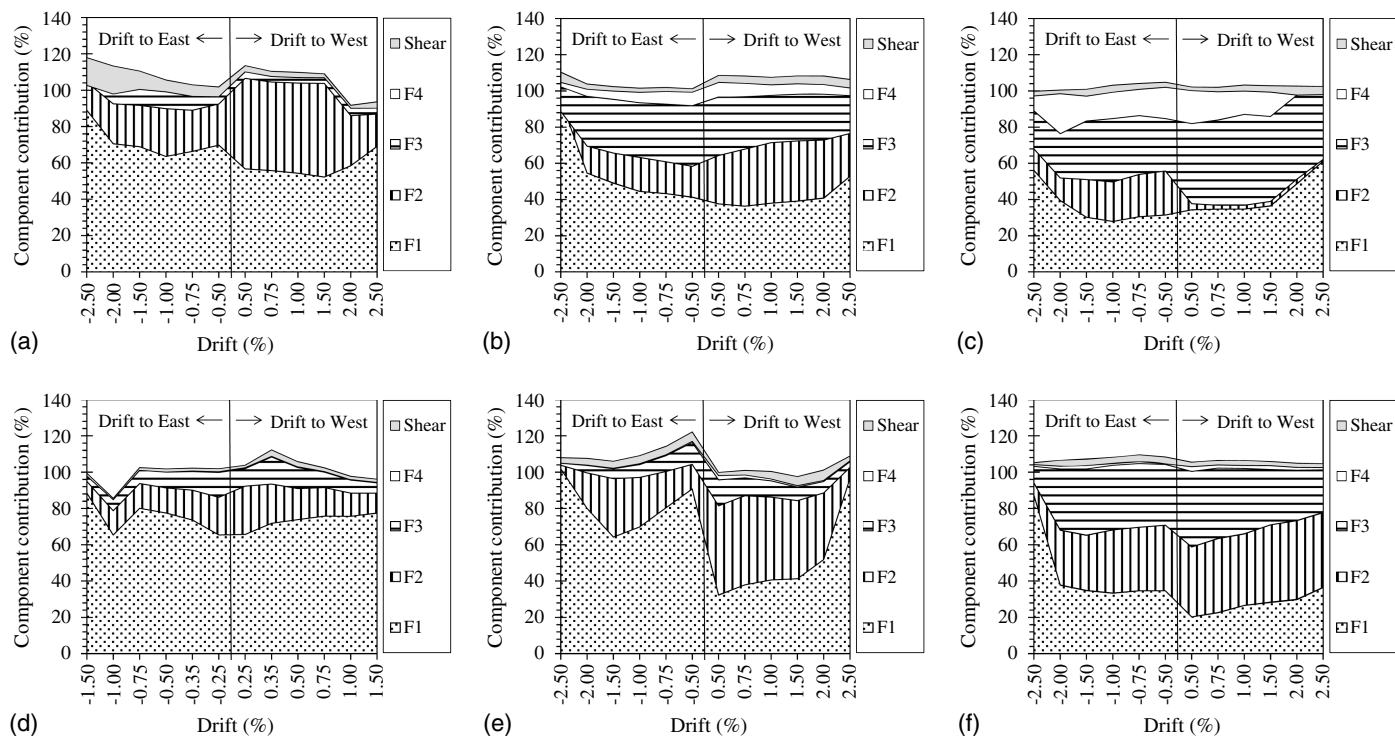


Fig. 10. Displacement components of all six test walls: (a) Wall C1; (b) Wall C2; (c) Wall C3; (d) Wall C4; (e) Wall C5; (f) Wall C6

C1, component F1, which accounts for one-fourteenth of the wall height, contributed nearly 60% of the total lateral displacement, and the combined F1 and F2 components, which account for one-sixth of the wall height, contributed almost 100% of the total lateral displacement. These local deformations confirmed that inelastic deformation was not distributed over a large length of the wall height and that the wall behavior was instead dominated by one or two main flexural cracks at the wall base. In addition, it can be observed that the relative contribution of F1 increased and the other flexural components decreased sharply between drifts of 2.0 and 2.5%. This concentration occurred as the dominant flexural crack at the wall base widened at large drifts, resulting in large inelastic strains and fracture of the vertical reinforcement. A typical example is Wall C6, where fracture of the vertical reinforcement occurred during the second cycle at -2.0% drift. The contributions of F1 and F2 to the lateral displacement respectively increased and decreased sharply from -2.0 to -2.5% drift. The components were asymmetric during some tests owing to differences in the crack distribution at each end of the wall.

The deformation components calculated also highlighted the difference in behavior between Walls C1, C2, and C3 with varied shear span ratios. In walls with a higher shear span ratio, the cracks extended higher up the wall and the upper sections of the wall panel contributed more to the wall lateral displacement. As shown in Fig. 10, components F3 and F4 accounted for nearly 25–40% of the lateral displacement in Walls C2, C3, and C6. For Wall C4 with no axial load, the lowest number of flexural cracks formed and the lateral deformation was primarily located in the bottom portion of the wall. As shown in Fig. 10(d), F1 contributed nearly 80% of the wall displacement in Wall C4. The contribution of deformation components in Walls C2 and C6 was similar, confirming that the transverse reinforcement detailing in the wall ends did not significantly affect the crack pattern or wall behavior.

Curvature Distribution

The average curvature distributions calculated from the displacement gauges up the wall height at the first cycle at each drift level for each test are shown in Fig. 11. Because the test walls were dominated by two to three large cracks, it was difficult to separate the strain penetration at the wall base from the widest flexural crack. Therefore, the curvature calculated adjacent to the foundation interface in Fig. 11 includes the reinforcement strain penetration. Furthermore, the value of this curvature at the wall base might be slightly underestimated since the prestressing of the foundation would increase the bond strength of the reinforcement and potentially reduce the strain penetration of the vertical reinforcement.

The curvature distributions further confirm the observed wall behavior and correlate well with the crack patterns shown in Fig. 7 and the deformation component in Fig. 10. Owing to a lack of secondary cracks, the curvature distribution for all six walls contained a few sharp curvature peaks at the location of wide cracks as opposed to continuously distributed curvatures over the wall height. The largest curvature peaks occurred at the wall base for all tests and further confirmed that the lateral deformation was concentrated at primary flexural cracks at the wall base. As expected, the curvature distribution was greatly influenced by the crack distribution. For Walls C2, C3, and C6 with higher shear span ratios, cracks extended higher up the wall height, and so the curvature distribution indicated peaks further up the wall. The largest curvature occurred at the wall base for all test walls except for Wall C6, where the largest curvature occurred slightly above the wall base and within the second layer of displacement gauges.

Plastic Hinge Length

For convenience of calculating the displacement capacity of RC members, an equivalent plastic hinge length (l_p) is usually defined over which the plastic hinge rotations are assumed to occur. The

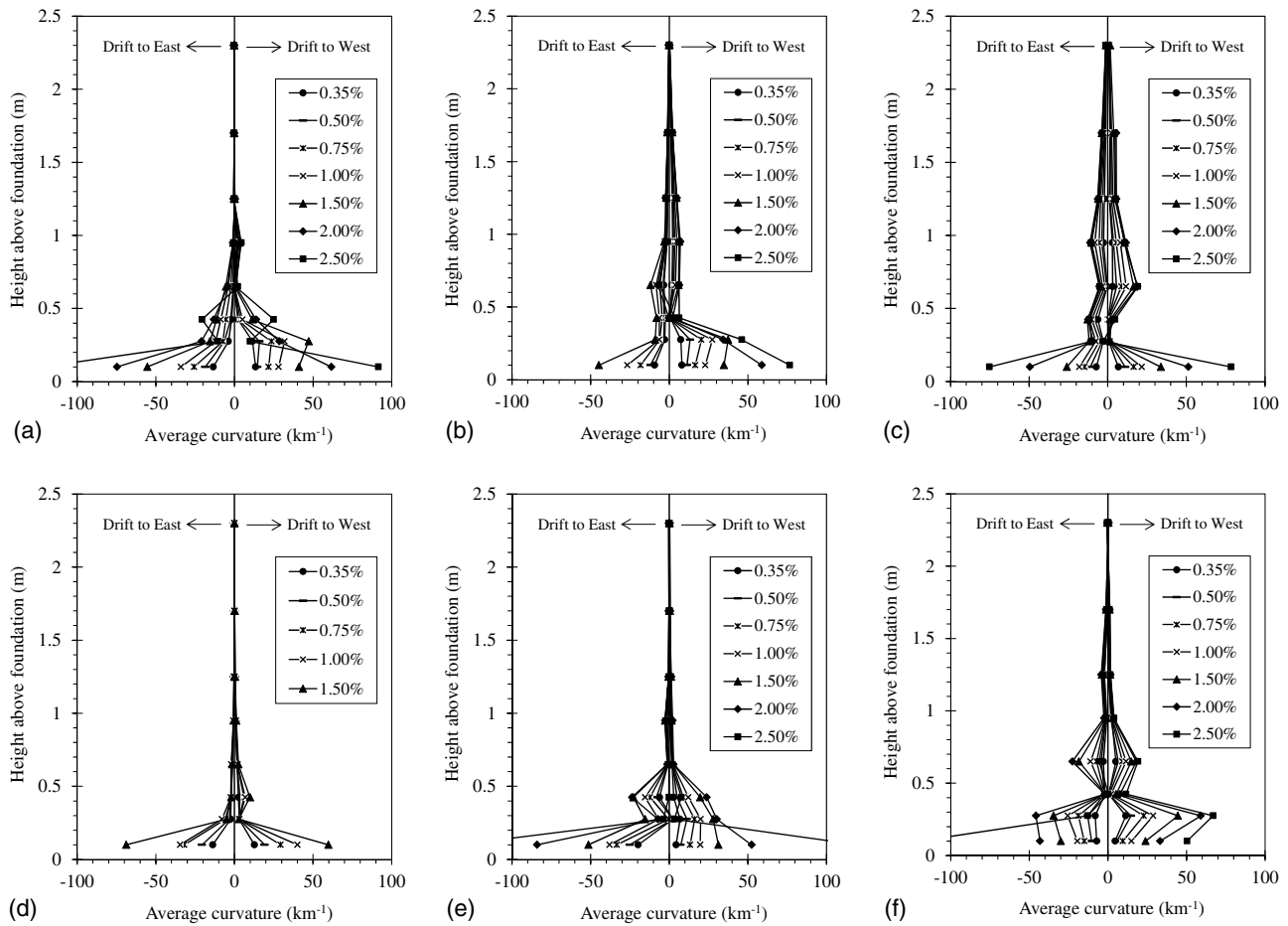


Fig. 11. Curvature distributions over height of all six test walls: (a) Wall C1; (b) Wall C2; (c) Wall C3; (d) Wall C4; (e) Wall C5; (f) Wall C6

plastic rotation (θ_p) was calculated by integrating the plastic curvature profile over the entire wall height, where the yield curvature was defined as $\varphi_y = 2\varepsilon_y/l_w$ (Priestley and Kowalsky 1998). The equivalent plastic hinge length was then calculated according to Eq. (2), where φ_m is the maximum curvature measured during the test:

$$\theta_p = (\varphi_m - \varphi_y)l_p \quad (2)$$

The l_p calculated at each drift cycle for each of the test walls are plotted alongside the theoretical l_p calculated in accordance with

NZS 3101:2006 in Fig. 12. In NZS 3101:2006, l_p is calculated as the smaller of $0.15M/V$ and $0.5l_w$, which is consistent with recommendations from previous researchers (Wallace and Orakcal 2002; Adebar et al. 2005). The NZS 3101 estimated l_p for the test walls with a shear span ratio of 2 was controlled by $0.15M/V$ (or 420 mm), while $0.5l_w$ (or 700 mm) governed for the test walls with a shear span ratio of 4 or 6. As shown in Fig. 12, the l_p calculated from the test data was typically well below the theoretical l_p owing to the low vertical reinforcement content and

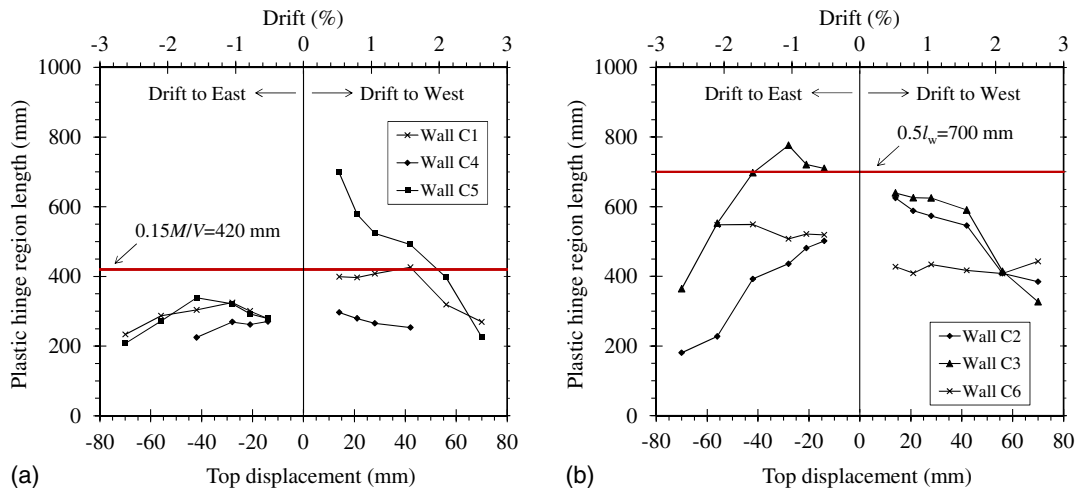


Fig. 12. Calculated plastic hinge lengths of test walls: (a) Walls C1, C4, and C5; (b) Walls C2, C3, and C6

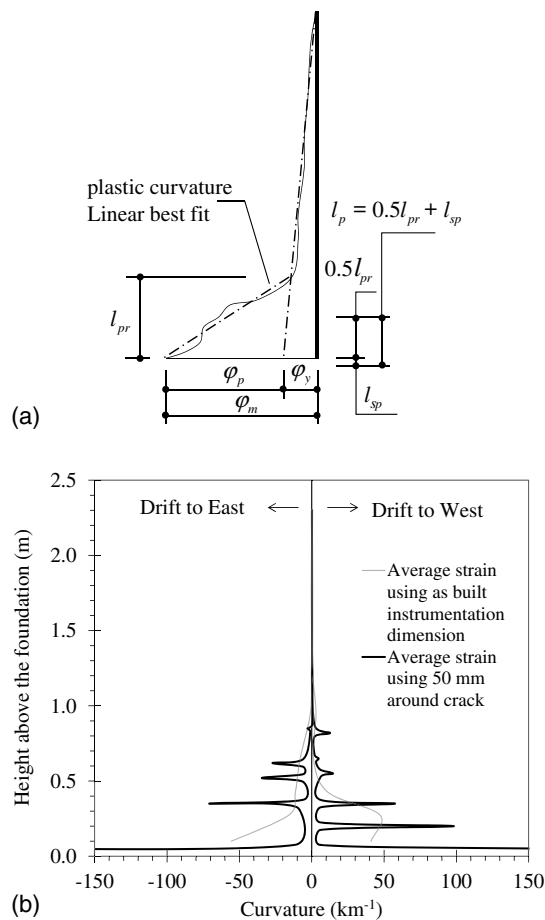


Fig. 13. Plastic hinge analysis methodology: (a) assumed plastic curvature distribution for plastic hinge analysis; (b) true curvature distribution of Wall C1 at 1.5% drift

decreased during large drift cycles because of the concentration of plasticity at a limited number of cracks. The average l_p calculated from the test data for Walls C1, C4, and C5 at drifts of $\pm 2.5\%$ was approximately 200 mm, less than half of the NZS 3101 estimated l_p of 420 mm for a wall with a shear span ratio of 2. For Walls C2, C3, and C6 at drifts of $\pm 2.5\%$, the average test l_p was approximately 700 mm, which is 43% less than the NZS 3101 estimated l_p of 400 mm for walls with a shear span ratio greater than 2.

Fig. 13(a) shows the typical curvature distribution observed for walls with well-detailed reinforcement, in which the inelastic curvatures usually vary linearly over the plastic hinge region (Hines et al. 2004; Bohl and Adebar 2011). Based on this assumption, l_p is usually taken as the summation of half the distance from the critical section to the point of contraflexure (l_{pr}) and the length of reinforcement strain penetration into the foundation (l_{sp}). However, for the test walls herein, the curvature over the wall was not evenly distributed but instead had sharp peaks at locations of flexural cracks. Because the average curvatures in the test walls were calculated based on a large gauge length of 150 mm, the measured curvature distributions in Fig. 11 appear somewhat linear at the wall base, despite the wall behavior's being dominated by one or two discrete cracks. If the gauge length over which the curvatures are averaged at each crack is assumed to be only 50 mm, the sharp peaks in the curvature distribution at the cracks are more obvious, as shown for Wall C1 in Fig. 13(b). Because of these strain and curvature concentrations at a discrete number of flexural cracks, it is concluded that the typical assumptions used to calculate plastic

hinge lengths are not valid for these test walls. This point is further highlighted by the scatter in both curvature distribution and calculated l_p values shown in Figs. 11 and 12, respectively. The l_p in the positive and negative loading directions was not symmetrical owing to the effect of different crack patterns. The traditional plastic hinge length methods of analysis may not be suitable for lightly reinforced concrete walls, making the calculation of ultimate drift based on curvature or rotation limits inaccurate.

Vertical Reinforcement Strains

The average tensile strains measured along the extreme vertical reinforcement up the height of the wall are plotted in Fig. 14 for each test wall. The strains were obtained by dividing the readings from the displacement gauges welded onto the vertical reinforcement as shown in Fig. 4(b) by the corresponding gauge length of 150 mm. Strain measurements were compromised after the reinforcement buckled, and so these values are not plotted in Fig. 14. Unlike well-detailed ductile RC walls where the reinforcement strains are evenly distributed over the plastic hinge length (Adebar et al. 2008; Dazio et al. 2009), the reinforcement strains in the test walls were inconsistent up the wall height, with inelastic strains concentrated at crack locations. Large reinforcement strains occurred at the wall base for all test walls, further confirming the concentrated inelastic deformations at one or two flexural cracks. The average strain measurements were significantly affected by the crack distribution, and the strain profiles were also dependent on the gauge length, as was highlighted for the calculated curvature profiles in Fig. 13(b). However, it was noted that as the shear span increased (e.g., Walls C1, C2, and C3) the vertical reinforcement yielded over a larger length of the wall height.

Reinforcement Buckling

As discussed earlier, the failure of all six test walls was controlled by buckling and subsequent fracture of the vertical reinforcement. Test Walls C1–C5 were originally designed for limited ductility requirements in accordance with NZS 3101:2006, which currently states that antibuckling reinforcement is only required when the vertical reinforcement ratio exceeds $3/f_y$ in limited ductile hinges or $2/f_y$ in ductile hinges (Clause 11.4.6.3). The commentary to this clause explains that in the critical flexural compression zone of walls, reinforcement buckling and concrete spalling are not expected to occur if the vertical reinforcement ratio is low. Similar provisions can also be found in ACI 318-14 (ACI 2014), which states that antibuckling ties are only required when the vertical reinforcement ratio exceeds $2.76/f_y$. In the case of the test walls, antibuckling ties were not required since the vertical reinforcement ratio of 0.53% was less than the limits set out in NZS 3101:2006 and ACI 318-14. However, during the tests of Walls C1, C2, C3, and C5, the vertical reinforcement buckled during cycles at 1.5% lateral drift. During the test of Wall C4 with no axial load, the vertical reinforcement buckled even earlier during cycles at 0.75% lateral drift. Based on these observations, it is not logical that walls with low vertical reinforcement contents are exempt from antibuckling ties. The wide cracks that form in these walls increase the concentration of inelastic strains in the vertical reinforcement, resulting in a strong likelihood of reinforcement buckling at moderate drifts.

Even when stirrups of R6 at 60 mm stirrups were placed in the toes of Wall C6, which was compliant with current antibuckling requirements of ductile hinges in NZS 3101:2006, the vertical reinforcement still buckled at relatively modest lateral drifts of 1.5 or 2%. This observation further highlights the vulnerability

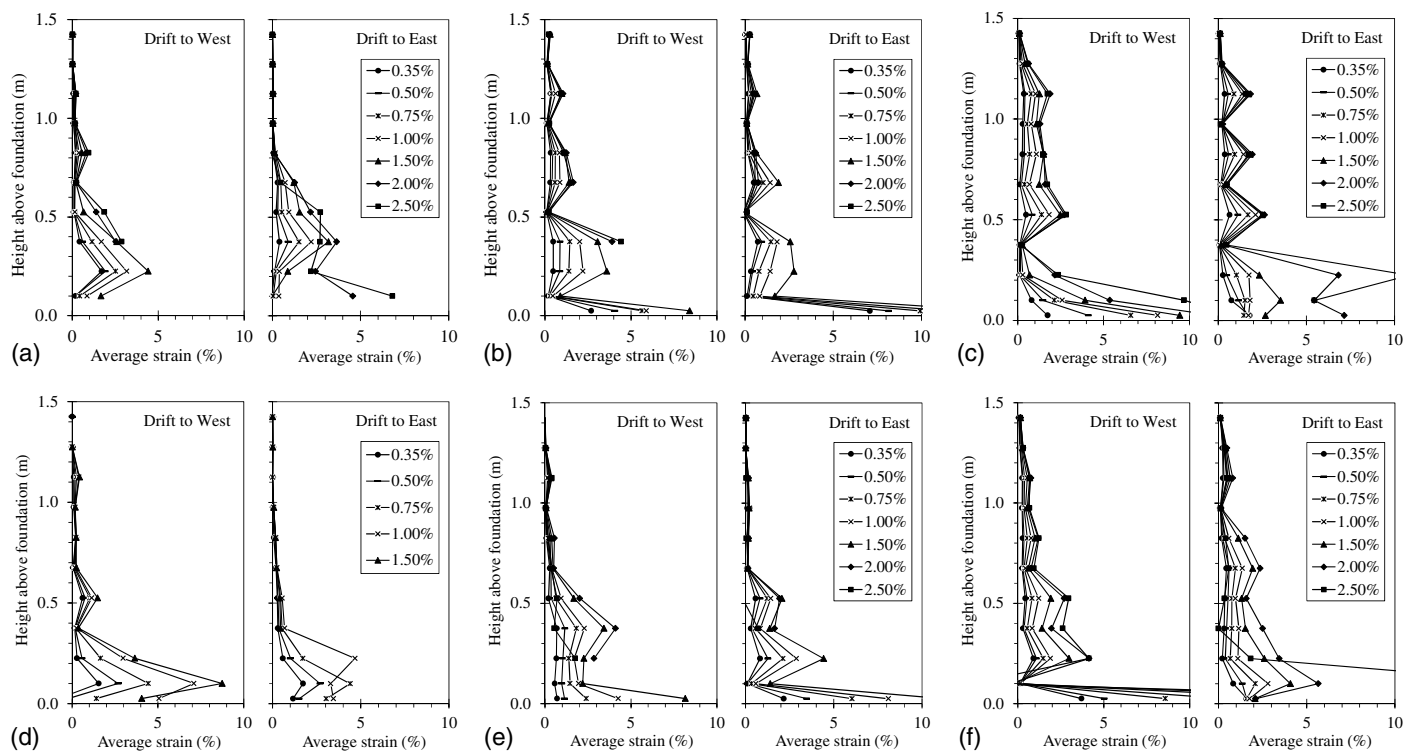


Fig. 14. Average strains along corner bars of all six test walls: (a) Wall C1; (b) Wall C2; (c) Wall C3; (d) Wall C4; (e) Wall C5; (f) Wall C6

of lightly reinforced concrete walls to the buckling of vertical reinforcement, and antibuckling ties may not have a significant impact on delaying the buckling. Analysing the results of all six wall tests, the measured reinforcement tensile strains in the cycle prior to buckling were investigated. The onset of reinforcement buckling was defined as visible distress during the test, typically in the form of the concrete spalling or vertical cracks initiating adjacent to the buckled reinforcement. As shown in Table 4, the average reinforcement tensile strain prior to buckling ranged from 2.2 to 4.5%, with an average of 3.5 and 3.3% for east and west ends of the wall, respectively. These large inelastic strains occurred at the location of the dominant flexural crack at the wall base, and the transverse reinforcement ties offered little restraint against the vertical reinforcement buckling as the wide crack opened and closed. The difference in reinforcement strains at each end of the wall was due to the difference in the crack distribution and widths at each end. The observed crack pattern and damage correlated well with the variation in measured strains. Increasing the vertical

Table 4. Vertical Reinforcement Tensile Strain at Reinforcement Buckling

Test wall	East end (%)	West end (%)
C1	4.4	2.2
C2	3.6	2.8
C3	2.6	3.5
C4	4.4	4.4
C5	8.2 ^a	2.9
C6	4.1	4.1
Average	3.8	3.3
COV	20%	25%

Note: COV = coefficient of variation.

^aBuckling occurred in a different location where the measuring length is only 50 mm; other steel strains are based on a gauge length of 150 mm. This value was not included when calculating the average value and the coefficient of variation.

reinforcement may help to delay buckling of the vertical reinforcement since an increased number of secondary cracks would allow the reinforcement strains to be more evenly distributed over the plastic hinge region.

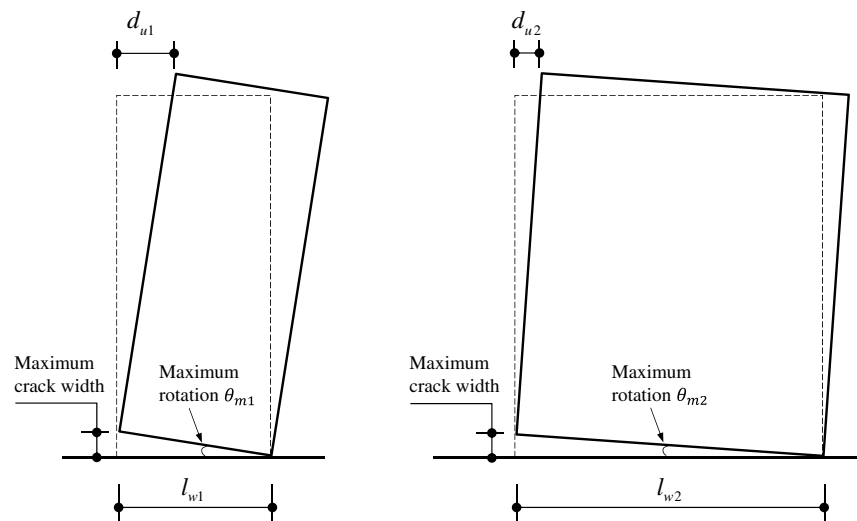
Cracking Moment

The measured and calculated moment capacities at the wall base are summarized in Table 5. The average concrete tensile strength given by the *fib* 2010 model code (*fib* 2013) was used for the calculated cracking moment (M_{cr_calc}) since it is considered to represent state-of-the-art knowledge on concrete properties and a more realistic expression for the average tensile strength compared to other design standards. The nominal flexural strength (M_n) was calculated based on a rectangular stress block using the specified concrete strength and lower characteristic yield strength of the reinforcement (as per NZS 3101:2006 and ACI 318:14). On average, the measured cracking moment (M_{cr_test}) was 19% larger than M_{cr_calc} . The average ratio of the measured flexural strength when the outermost vertical reinforcement first yielded (M_{y_test}) to the measured cracking moment (M_{cr_test}) was 1.15. In addition, the average ratio of the maximum flexural strength measured during the test (M_{max_test}) to M_{cr_test} was 1.57, indicating that a significant amount of strain hardening occurred in the reinforcement. Furthermore, the average ratio of the calculated nominal flexural strength (M_n) to the calculated average cracking moment (M_{cr_calc}) was 1.56. These ratios show that, although there was no sudden loss of strength following cracking, the margin of safety between yield strength and first cracking was small. In comparison, design provisions for minimum longitudinal reinforcement in RC beams has traditionally been based on a ratio of M_n to M_{cr} of at least 1.5 to 2.0 (Henry 2013). Despite the fact that all six test walls avoided a nonductile response with stable strength and strain hardening following cracking, they did not develop a large number of well-distributed flexural cracks. This observation indicates that

Table 5. Comparison of Cracking, Yield, and Maximum Moment of All Six Test Walls

Test wall	Direction	M_{cr_test} (kN · m)	M_{cr_calc} (kN · m)	M_{y_test} (kN · m)	M_{max_test} (kN · m)	M_n (kN · m)	$M_{cr_test}/$ M_{cr_calc}	$M_{y_test}/$ M_{cr_test}	$M_{max_test}/$ M_{cr_test}	$M_n/$ M_{cr_calc}
C1	+	332.5	236.2	352.9	485.7	404.3	1.41	1.06	1.46	1.71
	-	-319.3	-236.2	-406.9	-490.2	-404.3	1.35	1.27	1.54	1.71
C2	+	324.6	224.4	354.4	498.8	404.3	1.45	1.09	1.54	1.80
	-	-336.7	-224.4	-372	-479.2	-404.3	1.50	1.10	1.42	1.80
C3	+	304.8	229.5	327.5	474.5	404.3	1.33	1.07	1.56	1.76
	-	-332.3	-229.5	-356.9	-469.1	-404.3	1.45	1.07	1.41	1.76
C4	+	169.5	156.4	189.3	267.3	222.9	1.08	1.12	1.58	1.43
	-	-153.2	-156.4	-186.2	-246.4	-222.9	0.98	1.22	1.61	1.43
C5	+	415.4	292.7	498.4	664.4	554.6	1.42	1.20	1.60	1.89
	-	-345.5	-292.7	-507.9	-646.9	-554.6	1.18	1.47	1.87	1.89
C6	+	334.9	232.7	336.6	480.0	404.3	1.44	1.01	1.43	1.74
	-	-272.8	-232.7	-314.4	-504.6	-404.3	1.17	1.15	1.85	1.74
Average	—	—	—	—	—	—	1.31	1.15	1.57	1.72
COV	—	—	—	—	—	—	0.13	0.11	0.10	0.09

Note: COV = coefficient of variation; + signifies drift to west; - signifies drift to east.

**Fig. 15.** Single-crack model for lightly reinforced concrete walls

the M_n/M_{cr} criterion is only suitable for preventing sudden failure due to a loss of lateral strength after cracking. To achieve improved ductility for lightly reinforced concrete walls, the minimum vertical reinforcement provisions in NZS 3101:2006 need to be revised to include a criterion that ensures the development of well-distributed primary and secondary cracks in plastic hinge regions.

Drift Capacity

The ultimate drift capacity of the test walls was defined as the drift at which the strength was 20% below the maximum strength reached during the test (Park 1989). Based on this criterion, the drift capacity of Wall C4 with no axial load was 1.5%, and the drift capacity of the remaining five test walls was 2.5%, indicating that the wall achieved reasonable ductility despite the lack of distributed flexural cracking. However, the drift capacity observed for the test walls may be overestimated when compared to full-scale walls. The ultimate drift was significantly dependent on the ultimate strain of the reinforcing steel as drift capacity was controlled by reinforcement fracture for all tests. In accordance with New Zealand standards, the earthquake-grade G300E reinforcing bar used during the test must have a uniform elongation at maximum strength greater than 15% and a strain hardening ratio (f_u/f_y) larger than

1.15 [AS/NZS 4671 (AS/NZS 2001)]. Compared to higher-strength G500E reinforcement also manufactured in New Zealand or other reinforcing types overseas, G300E can be regarded as high-ductility reinforcing steel. For example, G500E reinforcement is only required to have a maximum uniform elongation of more than 10% [AS/NZS 4671 (AS/NZS 2001)], and reinforcing types Class A, B, and C in Eurocode 2 all have less ductility and strain hardening than G300E reinforcement [CEN 1992-1-1:2004 (CEN 2004)]. Using lower-ductility reinforcement would result in earlier reinforcement fracture and reduced drift capacity.

In addition to the reinforcement properties, the reinforcement fracture and wall drift capacity are strongly related to crack width. When the wall behavior is dominated by a discrete number of flexural cracks, plastic hinge rotation and the lateral drift at which certain crack widths occur will be a function of the wall length, as shown by the example in Fig. 15. Measurements of the crack widths during the wall tests suggested that maximum crack widths were consistently around 20 mm when the reinforcement fractured (Fig. 7). Note that reinforcement bar size will affect the strain penetration and, therefore, the crack width at fracture. A 10 mm bar was used in the test because it was the smallest deformed reinforcement available in New Zealand. However, this size bar did not accurately reflect the test wall scale since reinforcing bars of similar

size are still used in full-scale lightly reinforced concrete walls, such as the DH12 (12 mm bars) vertical reinforcement used in the Gallery apartment building in Christchurch (Smith and England 2012). Therefore, the maximum crack width at which the reinforcement fractures in a full scale walls may not be significantly larger than that used in the test walls. However, owing to the 40–50% scale of the walls tested, the length was only 1.4 m. If the wall length at full scale was twice that of the test wall, the drift capacity at which a 20 mm crack formed and reinforcement fracture occurred would be expected to be approximately half that of the scaled test wall, as shown in Fig. 15. Based on these findings, it is cautioned that the drift capacity of lightly reinforced concrete walls in real buildings may be significantly less than the 2.5% drift sustained by the scaled walls tested in the laboratory.

Conclusions

The test results of six RC walls designed in accordance with the minimum vertical reinforcement requirements in NZS 3101:2006 were presented. The test observations and results, including crack pattern, failure mode, and overall hysteric response, were presented and test data were discussed in terms of deformation components, curvature distribution, plastic hinge length, reinforcement strains, reinforcement buckling, cracking moment, and drift capacity. The main conclusions drawn from this experimental study are summarized as follows:

- The behavior of all six test walls was controlled by one to three large flexural cracks at the wall base. Cracks in walls with larger shear span ratios extended higher up the walls, but the overall behavior was still controlled by only one to three main cracks at the wall base. Neither the axial load nor the additional transverse reinforcement in the wall ends significantly affected the crack pattern observed.
- The curvature and reinforcement strain distributions in the plastic hinge region of the test walls were not linear and had several sharp peaks with concentrations of curvature and strain at the locations of large flexural cracks. The limited cracking greatly reduced the spread of the plasticity, and it was shown that typical plastic hinge length assumptions that are used to estimate curvature demands are inaccurate for lightly reinforced concrete walls.
- The failure for all six test walls was controlled by vertical reinforcement buckling and subsequent reinforcement fracture. The formation of wide cracks in the test walls was found to be the main reason for buckling of vertical reinforcement as the concentration of inelastic strains occurred in the vertical reinforcement. Antibuckling ties had no significant effect on delaying the buckling of vertical reinforcement, and it was concluded that lightly reinforced concrete walls are particularly vulnerable to reinforcement buckling at modest lateral drifts.
- The lateral drift capacity of the wall with no axial load was 1.5% and that of the other five walls were all 2.5%. The absence of axial load resulted in poor behavior and reduced the drift capacity compared to walls with a reasonable axial load. Both the shear span ratio and inclusion of transverse reinforcement ties in the ends of walls had no significant effect on the drift capacity of the test walls. The drift capacity of all walls was controlled by reinforcing bar fracture, and it was shown that the drift capacity of full-scale lightly reinforced concrete walls may be significantly less than that of the scaled test walls.
- The current minimum vertical reinforcement requirements for RC walls in NZS 3101:2006 (Amendment 2) are sufficient to prevent a sudden loss in strength after first cracking; however,

they are insufficient to ensure that a large number of secondary cracks will form in plastic hinge regions. Because the requirements in ACI 318-14 and Eurocode 8 typically result in less vertical reinforcement than that required by NZS 3101:2006, the behavior of comparable walls designed in accordance with other design standards may result in a further reduction in cracking and possibility of sudden loss in strength when the first flexural crack forms.

- It is recommended that the minimum vertical reinforcement requirement for ductile RC walls in all design standards should be reassessed to include a criterion that ensures the development of well-distributed cracks in plastic hinge regions.

Acknowledgments

Financial support for this research was provided by the Natural Hazards Research Platform through Contract C05X0907 in addition to the Chinese Scholarship Council and the University of Auckland. The assistance of Daniel Ripley, Jerome Quenneville, Mark Byrami, Ross Reichardt, Kimberley Twigden, Ash Jones, Ignáčák Miroslav, Pouya Seifi, Alex Shegay, Damien Duchet, Astrid Michard, and Theodore Carlos during the testing is greatly appreciated.

References

- ACI (American Concrete Institute). (2008). "Acceptance criteria for special unbonded post-tensioned precast structural walls based on validation testing and commentary." Farmington Hills, MI.
- ACI (American Concrete Institute). (2013). "Guide for testing reinforced concrete structural element under slowly applied simulated seismic loads." Farmington Hills, MI.
- ACI (American Concrete Institute). (2014). "Building code requirements for structural concrete (ACI 318-14) and commentary." *ACI 318-14*, Farmington Hills, MI.
- Adebar, P., Ibrahim, A. M. M., and Bryson, M. (2008). "Test of high-rise core wall: Effective stiffness for seismic analysis." *ACI Struct. J.*, 105(4), 509–512.
- Adebar, P., Mutrie, J., and DeVall, R. (2005). "Ductility of concrete walls: The Canadian seismic design provisions 1984 to 2004." *Can. J. Civ. Eng.*, 32(6), 1124–1137.
- AS (Standards Australia) and NZS (Standards New Zealand). (2001). "Steel reinforcing materials." *AS/NZS 4671*, Sydney, Australia, and Wellington, New Zealand.
- Bohl, A., and Adebar, P. (2011). "Plastic hinge lengths in high-rise concrete shear walls." *ACI Struct. J.*, 108(2), 148–157.
- Brueggen, B. L. (2009). "Performance of T-shaped reinforced concrete structural walls under multi-directional loading." Ph.D. thesis, Univ. of Minnesota, Ann Arbor, MI.
- Canterbury Earthquakes Royal Commission. (2012). "Final report: Volume 2: The performance of Christchurch CBD buildings." Wellington, New Zealand.
- CEN (European Committee for Standardization). (2004). "Eurocode 2: Design of concrete structures. Part 1-1: General rules and rules for buildings." *1992-1-1:2004*, Brussels, Belgium.
- CEN (European Committee for Standardization). (2004). "Eurocode 8: Design of structures for earthquake resistance." Brussels, Belgium.
- Crisafulli, F. J., Restrepo, J. I., and Park, R. (2002). "Seismic design of lightly reinforced precast concrete rectangular wall panels." *PCI J.*, 47(4), 104–121.
- Dazio, A., Beyer, K., and Bachmann, H. (2009). "Quasi-static cyclic tests and plastic hinge analysis of RC structural walls." *Eng. Struct.*, 31(7), 1556–1571.
- Deng, K., Pan, P., Shi, Y., Miao, Q., Li, W., and Wang, T. (2012). "Quasi-static test of reinforced concrete shear wall with low concrete strength and reinforcement ratio." Hong Kong.

- fib (Fédération Internationale du Béton). (2013). *fib model code for concrete structures 2010*, Wiley, Hoboken, NJ.
- Greifenhagen, C., and Lestuzzi, P. (2005). "Static cyclic tests on lightly reinforced concrete shear walls." *Eng. Struct.*, 27(11), 1703–1712.
- Han, S. W., Oh, Y. H., and Lee, L. H. (2002). "Seismic behaviour of structural walls with specific details." *Mag. Concr. Res.*, 54(5), 333–345.
- Henry, R. S. (2013). "Assessment of minimum vertical reinforcement limits for RC walls." *Bull. N.Z. Soc. Earthquake Eng.*, 46(2), 88–96.
- Hidalgo, P. A., Ledezma, C. A., and Jordan, R. M. (2002). "Seismic behavior of squat reinforced concrete shear walls." *Earthquake Spectra*, 18(2), 287–308.
- Hines, E. M., Restrepo, J. I., and Seible, F. (2004). "Force-displacement characterization of well-confined bridge piers." *ACI Struct. J.*, 101(4), 537–548.
- Hiraishi, H. (1984). "Evaluation of shear and flexural deformations of flexural type shear walls." *Bull. N.Z. Natl. Soc. Earthquake Eng.*, 17(2), 135–144.
- Kam, W. Y., Pampanin, S., and Elwood, K. J. (2011). "Seismic performance of reinforced concrete buildings in the 22 February Christchurch (Lyttelton) earthquake." *Bull. N.Z. Soc. Earthquake Eng.*, 44(4), 239–278.
- Li, B., Pan, Z., and Xiang, W. (2012). "Experimental evaluation of seismic performance of squat RC structural walls with limited ductility reinforcing details." *J. Earthquake Eng.*, 19(2), 313–331.
- Lowes, L. N., Lehman, D. E., Birely, A. C., Kuchma, D. A., Marley, K. P., and Hart, C. R. (2012). "Earthquake response of slender planar concrete walls with modern detailing." *Eng. Struct.*, 43, 31–47.
- NZS (Standards New Zealand). (1986). "Methods of test for concrete. Part 2: Tests relating to the determination of strength of concrete." Wellington, New Zealand.
- NZS (Standards New Zealand). (2006). "Concrete structures standard (Amendment 2)." Wellington, New Zealand.
- Park, R. (1989). "Evaluation of ductility of structures and structural assemblages from laboratory testing." *Bull. N.Z. Nat. Soc. Earthquake Eng.*, 22(3), 155–166.
- Priestley, M. J. N., and Kowalsky, M. J. (1998). "Aspects of drift and ductility capacity of rectangular cantilever structural walls." *Bull. N.Z. Natl. Soc. Earthquake Eng.*, 31(2), 73–85.
- SESOC (Structural Engineering Society of New Zealand). (2011). "Preliminary observations from Christchurch earthquakes." (<http://canterbury.royalcommission.govt.nz/documents-by-key/20111205.1533>) (Dec. 5, 2011).
- Smith, P., and England, V. (2012). "Independent assessment on earthquake performance of Gallery Apartments—62 Gloucester Street." Canterbury Earthquakes Royal Commission, Wellington, New Zealand.
- Sritharan, S., Beyer, K., Henry, R. S., Chai, M., and Bull, D. (2014). "Understanding poor seismic performance of concrete walls and design implications." *Earthquake Spectra*, 30(1), 307–334.
- Wallace, J. W., and Orakcal, K. (2002). "ACI 318-99 provisions for seismic design of structural walls." *ACI Struct. J.*, 99(4), 499–508.
- Wood, S. L. (1989). "Minimum tensile reinforcement requirements in walls." *ACI Struct. J.*, 86(5), 582–591.
- Wood, S. L., Stark, R., and Greer, S. A. (1991). "Collapse of eight-story RC building during 1985 Chile earthquake." *J. Struct. Eng.*, 10.1061/(ASCE)0733-9445(1991)117:2(600), 600–619.